NASA/CR-1999-209825
ICASE Report No. 99-48

On Aeroacoustics of a Stagnation Flow Near a Rigid Wall

Alex Povitsky
ICASE, Hampton, Virginia

Institute for Computer Applications in Science and Engineering
NASA Langley Research Center
Hampton, VA

Operated by Universities Space Research Association

National Aeronautics and
Space Administration

Langley Research Center
Hampton, Virginia 23681-2199

Prepared for Langley Research Center
under Contract NAS1-97046

December 1999

ON AEROACOUSTICS OF A STAGNATION FLOW NEAR A RIGID WALL

ALEX POVITSKY*

Abstract. We consider propagation of disturbances in a non-uniform mean flow by high-order numerical simulation. Monopole and dipole acoustic, vortical and entropy pulses are embedded in an incompressible stagnation flow, which is taken as a prototype of a non-uniform low Mach number mean flow near a rigid wall at high angle of attack.

Numerical results are discussed in terms of baroclinic generation of disturbance vorticity that appear to be a key process in energy transfer between a non-uniform mean flow and a propagating disturbance. These phenomena lead to amplification of sound waves originated from an acoustic pulse. Vorticity generation governs wave radiation of a near-wall entropy pulse and makes the radiated waves similar to those from a vortical dipole. Interaction of initial pulse vorticity with generated vorticity leads to various radiated wave patterns discussed here.

Key words. aeroacoustics of non-uniform flows, stagnation flow, wave amplification, vortical flows, monopole and dipole sources, high-order numerical simulation

Subject classification. Fluid Mechanics, Applied Mathematics

1. Introduction. Many practical problems in aeroacoustics that involve noise generation and propagation are actually problems of propagation of disturbances in a non-uniform mean flow. In this study we simulate numerically propagation of acoustic, vortical and entropy dipole and monopole pulses in a non-uniform incompressible mean flow and reflection of these disturbances by a solid wall. Stagnation flow is a special case of mean flow that mimics many practical problems in aeroacoustics, such as noise from a leading edge of an airfoil or a turbine blade, jet impingement noise in STOL/VTOL aircraft concept and engine noise.

Recent large-scale direct or acoustic analogy simulations for aeroacoustics of bodies suggested that the presence of strong mean flow gradients makes it extremely difficult to identify acoustic waves [12]. Slimon et al. [15] considered aeroacoustics of a flow past a circular cylinder with low Mach number and observed poor coincidence of their numerical computations with experimental data near the cylinder axis. Authors [15] used a CAA scheme called *expansion about incompressible flow* (EIF) developed by Hardin and Pope [5]. This approach splits an incompressible flow problem and a perturbation problem and does not allow the influence of the perturbation problem on the mean flow.

Strong amplification of noise by impingement of a jet upon a flat rigid bound was studied experimentally by Olsen et al. [14], Soderman [16] and Norus [13].

On the other hand, available numerical studies about a single disturbance propagation are devoted to propagation in a static environment, in uniform flows and in unidirectional sheared mean flows using either Lighthill acoustic analogy approach [11], [3] or numerical solution of Euler equations for given pulses [6], [17], [8]. For essentially non-uniform flows, Atassi and Grzedzinski [1] suggest to split the disturbance velocity into three components that significantly simplifies computations and reduces the governing equations to a

*Staff Scientist, ICASE, NASA Langley Research Center, Hampton, VA 23681-2199 (e-mail: aeralpo@icase.edu). This research was supported by the National Aeronautic and Space Administration under NASA Contract No. NAS1-97046 while the author was in residence at the Institute for Computer Applications in Science and Engineering (ICASE), NASA Langley Research Center, Hampton, VA 23681-2199

single Poisson equation. This study is applied to 3-D stagnation flows around bluff bodies with isolated stagnation points and represents an extention of M. Goldstein [4] approach to streaming motions with small unsteady disturbances. However, according to [1] this approach is not applicable to 2-D flows, having a stagnation line along the body surface.

Thus, detailed numerical investigation of a disturbance propagating in a non-uniform mean flow near stagnation point is needed. To obtain governing equations, the Euler equations are written in terms of the sum of known flowfield for the stagnation flow and unknown disturbance variables. These equations are solved numerically by high-order compact discretisation on a structured grid in the space-time domain. We study propagation of single pulses as it represents a building block for propagation of more complex disturbances in turbulent flows. Geometrically a stagnation flow is a relatively small spatial extent embedded in a uniform flow or in a static ambient medium; therefore, the data obtained is useful for far-field computations of radiated sound by integral methods.

The stagnation flow stretches acoustic, vorticity and density pulses and affects the intensity, shape, direction of propagation and profile of propagating waves. Near-field wave solutions in the stagnation flow appear to be very different from those obtained in a uniform flow or in a static environment. The goal of this study is to gain theoretical and computational insight into the governing physical mechanisms.

The article contains five sections. In the second section, the linearized Euler equations about the steady mean flow are obtained, the numerical procedure and artificial boundary conditions are described. In Section 3, results on the propagation of acoustic pulses in stagnation flow are presented. The obtained reflected waves are discussed in comparison with their counterparts for the static ambient medium. We show that baroclinic generation of vorticity controls the energy transfer between the mean stagnation flow and acoustic disturbance. In Section 4, the numerical results for vorticity monopole and dipole pulses are presented and a different scenario of near-wall vortex stretching and corresponding emission of acoustic waves is considered. Production of non-symmetric waves due to propagation and reflection of combined vorticity/entropy pulses is modeled. Section 5 contains results about propagation of entropy pulses in stagnation mean flow. An analogy between generation of waves originated from an entropy monopole pulse and from a vortical dipole is drawn in this section.

2. Governing equations and numerical procedure.

2.1. Euler equations for small disturbances. The two-dimensional unsteady Euler equations of ideal gas dynamics describe an inviscid flow in conservative form and can be written as:

$$\boldsymbol{q}_t + \boldsymbol{f}_x + \boldsymbol{g}_y = 0. \tag{1}$$

The vectors in equation (1) are

$$\boldsymbol{q} = \begin{pmatrix} \rho \\ \rho u \\ \rho v \\ e \end{pmatrix}, \ \boldsymbol{f} = \begin{pmatrix} \rho u \\ \rho u^2 + p \\ \rho uv \\ (e+p)u \end{pmatrix}, \ \boldsymbol{g} = \begin{pmatrix} \rho v \\ \rho uv \\ \rho v^2 + p \\ (e+p)v \end{pmatrix}, \tag{2}$$

where ρ is density, p is static pressure, (u, v) is velocity in Cartesian coordinates (x, y), and e is the total energy, related to the other variables by an equation of state, which, for a perfect gas, is

$$e = \frac{p}{(\gamma - 1)} + \frac{1}{2}\rho(u^2 + v^2) \tag{3}$$

where $\gamma = 1.4$ is the ratio of specific heats.

Consider velocities as sums of steady mean flow and acoustic disturbances

$$u = U + u\prime, v = V + v\prime, p = P + p\prime, \rho = 1 + \rho\prime. \tag{4}$$

We assume that the normalized speed of sound $c = \sqrt{\gamma p/\rho} = 1$ and, therefore, pressure and density obey the same equation. For simplicity, we omit $\prime$s in the following equations in this subsection. The Euler equations, presented in terms of mean flow variables and their disturbances, are given by

$$\begin{aligned}
(1+\rho)\frac{\partial(U+u)}{\partial t} &= -\frac{\partial(P+p)}{\partial x} - (U+u)(1+\rho)\frac{\partial(U+u)}{\partial x} - (V+v)(1+\rho)\frac{\partial(U+u)}{\partial y}, \\
(1+\rho)\frac{\partial(V+v)}{\partial t} &= -\frac{\partial(P+p)}{\partial y} - (U+u)(1+\rho)\frac{(\partial(V+v)}{\partial x} - (V+v)(1+\rho)\frac{\partial(V+v)}{\partial y}, \\
\frac{\partial(1+\rho)}{\partial t} &= -\frac{\partial((1+\rho)(U+u))}{\partial x} - \frac{\partial((1+\rho)(V+v))}{\partial y}.
\end{aligned} \tag{5}$$

If a mean flow is described by the irrotational flow model in the region between two straight zero-flux boundaries intersecting at an angle π/n [2], the stream-function field is given by

$$\psi = Ar^n sin(n\theta), \tag{6}$$

where (r, θ) are polar coordinates. Thus, this study can be easily expanded to any angle of attack.

In the special case $n = 2$ (stagnation flow) the velocity field is described by

$$U(x,y) = -2Ax, V(x,y) = 2Ay,\ A > 0. \tag{7}$$

For stagnation mean flow with a normalization leading to $2A = 1$, the linearized version of system (5) is obtained by neglecting second-order products of fluctuation quantities (such as $uv, \rho u, v^2$, and u^2) :

$$\begin{aligned}
\frac{\partial u}{\partial t} &= -\frac{\partial p}{\partial x} + x\frac{\partial u}{\partial x} + u - y\frac{\partial u}{\partial y} - x\rho \\
\frac{\partial v}{\partial t} &= -\frac{\partial p}{\partial y} - y\frac{\partial v}{\partial y} + x\frac{\partial v}{\partial x} - v - y\rho, \\
\frac{\partial \rho}{\partial t} &= -\frac{\partial u}{\partial x} - \frac{\partial v}{\partial y} + x\frac{\partial \rho}{\partial x} - y\frac{\partial \rho}{\partial y}.
\end{aligned} \tag{8}$$

Non-linear aeroacoustic equations for the stagnation mean flow are given by:

$$\begin{aligned}
\frac{\partial u}{\partial t} &= \left(-\frac{\partial p}{\partial x} + x\frac{\partial u}{\partial x} + u - y\frac{\partial u}{\partial y} - x\rho + \frac{\partial u}{\partial x}(x\rho - u - \rho u) + \rho u - \frac{\partial u}{\partial y}(y\rho + v + \rho v)\right)/(1+\rho) \\
\frac{\partial v}{\partial t} &= \left(-\frac{\partial p}{\partial y} - y\frac{\partial v}{\partial y} + x\frac{\partial v}{\partial x} - v - y\rho + \frac{\partial v}{\partial x}(x\rho - u - \rho u) - \rho v - \frac{\partial v}{\partial y}(y\rho + v + \rho v)\right)/(1+\rho) \\
\frac{\partial \rho}{\partial t} &= -\frac{\partial u}{\partial x} - \frac{\partial v}{\partial y} + x\frac{\partial \rho}{\partial x} - y\frac{\partial \rho}{\partial y} - \frac{\partial \rho u}{\partial x} - \frac{\partial \rho v}{\partial y}.
\end{aligned} \tag{9}$$

2.2. Numerical procedure. The spatial derivatives in Eqs. (8) and (9) are approximated using compact finite difference schemes [10]:

$$\beta U'_{i-2} + \alpha U'_{i-1} + U'_i + \alpha U'_{i+1} + \beta U'_{i+2} = \frac{a}{2\Delta x}(U_{i+1} - U_{i-1}) + \frac{b}{2\Delta x}(U_{i+2} - U_{i-2}), \tag{10}$$

where U' is the unknown derivative, Δx is the grid step and $U_{i-2}, ..., U_{i+2}$ denote values of variable U at grid nodes $i-2, ..., i+2$. In this study the classical Padé scheme ($\alpha = 0.25,\ a = 1.5$ and $\beta = b = 0$) with a

tridiagonal matrix for the right and left sides of (10) is used. One-side near-boundary spatial discretizations have the form

$$U_1' + \alpha_b U_2' = \frac{1}{\Delta x} \sum_{i=1,..,N_b} a_{bi} U_i, \tag{11}$$

where N_b is the size of the near-boundary stencil and a_{bi} are discretized coefficients. With this choice the boundary schemes can be used with a tridiagonal interior scheme without increasing the bandwidth [10].

Eqs. (8) and (9) are discretized in time with an explicit fourth-order Runge-Kutta (RK) scheme. The solution is advanced from time level n to time level $n+1$ in five sub-stages using a low-storage RK scheme proposed by Williamson [18] and implemented by Wilson et al. [19]:

$$\begin{aligned} H^M &= S_x \frac{\partial U^M}{\partial x} + S_y \frac{\partial U^M}{\partial y} + S_z \frac{\partial U^M}{\partial z} + a^M H^{M-1}, \\ U^{M+1} &= U^M + b^{M+1} \Delta t H^M, \end{aligned} \tag{12}$$

where M is the particular stage number; and the coefficients a^M and b^M depend upon the order of the RK scheme.

To provide grid refinement study, the computational domain $\Omega = [0 < x < 1.2] \times [-1.2 < y < 1.2]$ is covered with $80 \times 80, 120 \times 120$ and 160×160 uniform numerical grids. Centerline pressure profiles for these grids at time moment $t = 0.5$ are shown in Figure 1. The pressure profile for coarse grid 80×80 has small oscillations ahead the wave front and numerical local maximum near the stagnation point. Finer grid computations are free from these drawbacks and are practically identical for 120×120 and 160×160 grids; therefore, the 120×120 uniform numerical grid is used in this study. Time step is computed by $\Delta t = C \Delta x$, where the Courant number (C) is taken equal to 0.02.

At all boundaries but the flat plate, characteristic outflow boundary conditions [7] are applied. The mean flow is supersonic at the outflow boundaries; therefore, all numerical near-boundary disturbances should be moved out. Spatial discretizations at the outflow boundaries are computed by (11). For propagation of a pulse in the static environment, perfect matching layer (PML) [8] with thickness of ten grid nodes is implemented to suppress disturbances originated from boundary conditions.

At the flat plate ($x = 0$) reflection boundary conditions $\phi_b = \phi_{b-1}$ are used for pressure and velocity component v. For these variables, zero boundary conditions for spatial derivatives $\phi_b' = 0$ are used instead of approximation (11). Normal velocity u is equal to zero at this boundary and approximation (11) is implemented for its spatial derivative.

The computational procedure for this numerical method is as follows:

1. Compute the right-hand side of equations (10) using values of the governing variable U from the previous time step.
2. Compute the spatial derivatives solving tridiagonal systems in x and y spatial directions.
3. Compute the right-hand side of equations (8) or (9) using the spatial derivatives computed on Step 2 and update governing variables by Runge-Kutta scheme.
4. Compute boundary values of governing variables using characteristic and reflection boundary conditions.
5. Repeat computational steps 1-4 for all stages of Runge-Kutta scheme.
6. Repeat computational steps 1-5 for all time steps.

Numerical computations show that non-linear equations (9) give the same results as linearized equations (8).

3. Propagation of acoustic pulses. Reflection and propagation of an acoustic pulse in the stagnation mean flow (case A) in comparison with its propagation in the static ambient conditions in presence of wall (case B) are studied in this section. We solve numerically the system (9) by algorithm described in the previous section. Initial conditions describing this pulse are widely used in test aeroacoustic computations [6]:

$$p = \rho = \epsilon \exp\left[-d^2 \frac{(x-x_c)^2 + (y-y_c)^2}{a}\right], \tag{13}$$

where $\epsilon = 0.01, a = ln(2)/9, d = 60$ is the normalization coefficient, and the pulse is centered at ($x_c = 0.25, y_c = 0$).

In Figure 2 pressure fields are presented side by side for cases A (left column) and B (right column) at the same time moments. In case A, the mean flow stretches the pulse in the y direction and compresses it in the x direction. In both cases, a reflected waves is formed; however, in case A the wave propagation upstream of the mean flow leads to formation of flat waves (Figure 2b,c). Maximum pressure is larger in case A than that in case B except the earlier time moment $t = .33$ (see Legend in Figure 2). Acoustic pulse propagates with the speed of sound relative to mean flow; therefore, propagation speed in steady frame (x, y) in case A is slower than that in case B.

Centerline profiles of pressure for the cases A and B at time moments $t = 0.165, 0.33, 0.495$ and 0.66 are shown in Figure 3. The acoustic pressure amplitude is almost constant in time in case A (Figure 3a), whereas in case B (Figure 3b) it decreases with the distance from the origin. For example, at $t = 0.66$ (curve 4 in Figure 3) the wave amplitude in case A is approximately two times larger than that in case B.

Thus, our aim is to understand the transfer of energy between the mean stagnation flow and a disturbance, that causes amplification of the pulse in case A as opposed to case B.

Let us rewrite Eq. (2) in terms of vorticity transport [7], [20]:

$$\frac{D}{Dt}(\frac{\omega}{\rho}) = \frac{1}{\rho}(\boldsymbol{\omega} \cdot \nabla \boldsymbol{u}) + \frac{1}{\rho^3}(\nabla\rho \times \nabla p) \tag{14}$$

$$\frac{D\rho}{Dt} = -\rho \nabla \boldsymbol{u}, \tag{15}$$

where $\rho, \boldsymbol{u} = (u, v)$ and P satisfy Eq. (4) and vorticity $\boldsymbol{\omega} = \boldsymbol{\omega\prime} + \boldsymbol{\Omega}$. In the 2-D case $\boldsymbol{\omega} = (0, 0, \omega)$, the term $\boldsymbol{\omega} \cdot \nabla \boldsymbol{u} = 0$, and Eq. (14) becomes

$$\rho \frac{D\omega}{Dt} + \omega \frac{D\rho}{Dt} = \frac{1}{\rho}(\nabla\rho \times \nabla p). \tag{16}$$

The right-hand side of above Eq. is transformed as follows:

$$\frac{1}{\rho}(\nabla\rho \times \nabla p) = (1 - \rho\prime)\nabla\rho\prime \times (\nabla P + \nabla p\prime) = \nabla\rho\prime \times \nabla P. \tag{17}$$

It should be noted, that $1/(1+\rho\prime) = 1 - \rho\prime + O(\rho\prime^2)$, the mean flow is irrotational ($\Omega = 0$) and incompressible ($\nabla \boldsymbol{U} = 0$), and $\nabla\rho\prime \times \nabla p\prime = 0$ for acoustic disturbances. We neglect the second-order terms $\omega\prime\rho\prime, u\prime\rho\prime$ in the left-hand side of Eq. (14) and in Eq. (15), to obtain

$$\frac{D\omega\prime}{Dt} = \nabla\rho\prime \times \nabla P \tag{18}$$

$$\frac{D\rho\prime}{Dt} = -\nabla \boldsymbol{u\prime}. \tag{19}$$

3. Propagation of acoustic pulses. Reflection and propagation of an acoustic pulse in the stagnation mean flow (case A) in comparison with its propagation in the static ambient conditions in presence of wall (case B) are studied in this section. We solve numerically the system (9) by algorithm described in the previous section. Initial conditions describing this pulse are widely used in test aeroacoustic computations [6]:

$$p = \rho = \epsilon \exp\left[-d^2 \frac{(x-x_c)^2 + (y-y_c)^2}{a}\right], \tag{13}$$

where $\epsilon = 0.01, a = ln(2)/9, d = 60$ is the normalization coefficient, and the pulse is centered at $(x_c = 0.25, y_c = 0)$.

In Figure 2 pressure fields are presented side by side for cases A (left column) and B (right column) at the same time moments. In case A, the mean flow stretches the pulse in the y direction and compresses it in the x direction. In both cases, a reflected waves is formed; however, in case A the wave propagation upstream of the mean flow leads to formation of flat waves (Figure 2b,c). Maximum pressure is larger in case A than that in case B except the earlier time moment $t = .33$ (see Legend in Figure 2). Acoustic pulse propagates with the speed of sound relative to mean flow; therefore, propagation speed in steady frame (x, y) in case A is slower than that in case B.

Centerline profiles of pressure for the cases A and B at time moments $t = 0.165, 0.33, 0.495$ and 0.66 are shown in Figure 3. The acoustic pressure amplitude is almost constant in time in case A (Figure 3a), whereas in case B (Figure 3b) it decreases with the distance from the origin. For example, at $t = 0.66$ (curve 4 in Figure 3) the wave amplitude in case A is approximately two times larger than that in case B.

Thus, our aim is to understand the transfer of energy between the mean stagnation flow and a disturbance, that causes amplification of the pulse in case A as opposed to case B.

Let us rewrite Eq. (2) in terms of vorticity transport [7], [20]:

$$\frac{D}{Dt}(\frac{\omega}{\rho}) = \frac{1}{\rho}(\boldsymbol{\omega} \cdot \nabla \boldsymbol{u}) + \frac{1}{\rho^3}(\nabla\rho \times \nabla p) \tag{14}$$

$$\frac{D\rho}{Dt} = -\rho \nabla \boldsymbol{u}, \tag{15}$$

where $\rho, \boldsymbol{u} = (u, v)$ and P satisfy Eq. (4) and vorticity $\boldsymbol{\omega} = \boldsymbol{\omega\prime} + \boldsymbol{\Omega}$. In the 2-D case $\boldsymbol{\omega} = (0, 0, \omega)$, the term $\boldsymbol{\omega} \cdot \nabla \boldsymbol{u} = 0$, and Eq. (14) becomes

$$\rho \frac{D\omega}{Dt} + \omega \frac{D\rho}{Dt} = \frac{1}{\rho}(\nabla\rho \times \nabla p). \tag{16}$$

The right-hand side of above Eq. is transformed as follows:

$$\frac{1}{\rho}(\nabla\rho \times \nabla p) = (1 - \rho\prime)\nabla\rho\prime \times (\nabla P + \nabla p\prime) = \nabla\rho\prime \times \nabla P. \tag{17}$$

It should be noted, that $1/(1+\rho\prime) = 1 - \rho\prime + O(\rho\prime^2)$, the mean flow is irrotational ($\Omega = 0$) and incompressible ($\nabla \boldsymbol{U} = 0$), and $\nabla\rho\prime \times \nabla p\prime = 0$ for acoustic disturbances. We neglect the second-order terms $\omega\prime\rho\prime, u\prime\rho\prime$ in the left-hand side of Eq. (14) and in Eq. (15), to obtain

$$\frac{D\omega\prime}{Dt} = \nabla\rho\prime \times \nabla P \tag{18}$$

$$\frac{D\rho\prime}{Dt} = -\nabla \boldsymbol{u\prime}. \tag{19}$$

Two fluid mechanics phenomena govern the process of pulse propagation: (i) the baroclinic generation of acoustic vorticity due to the interaction of mean field pressure gradient with density gradient of aeroacoustic disturbance; and (ii) the volume expansion of the disturbance. Note, that the former phenomenon exist only in a non-uniform flow, where the pressure gradient is not equal to zero, whereas the latter one is characteristic for any mean flow including static ambient conditions.

Equation of conservation of an acoustic energy density for irrotational and incompressible mean flow and adiabatic acoustic disturbance is given by [3]:

$$\frac{\partial E}{\partial t} + \nabla \boldsymbol{I} = \boldsymbol{u\prime} \cdot (\boldsymbol{U} \times \boldsymbol{\omega\prime}), \tag{20}$$

where $E = p\prime^2/2 + \boldsymbol{u\prime}^2/2 + \rho\prime \boldsymbol{u\prime} \cdot \boldsymbol{U}$ is the acoustic energy density and $\boldsymbol{I} = (p\prime + \boldsymbol{u\prime} \cdot \boldsymbol{U})(\boldsymbol{u\prime} + \rho\prime \boldsymbol{U})$ is the acoustic energy flux. For an irrotational source-free disturbance field, acoustic energy density is conserved, i.e., the net flux of acoustic energy across any surface is equal to time rate of change of energy within volume that this surface encloses [3]. On the contrary, for rotational disturbance field the acoustic energy is affected by the baroclinic generation of disturbance vorticity. In case of 2-D stagnation mean flow, the right side of Eq. (20) is expressed by:

$$\boldsymbol{u\prime} \cdot (\boldsymbol{U} \times \boldsymbol{\omega\prime}) = yu\omega + xv\omega. \tag{21}$$

Thus, the role of vorticity as an agent in energy transfer between the mean flow and disturbance is shown. Fields of the baroclinic vorticity generation $\nabla\rho\prime \times \nabla P$ and disturbance energy generation (21) are shown in Figure 4. The latter term is negative before the pulse hits the rigid wall ($t = 0.17$, Figure 4a) and positive when acoustic waves propagate opposite to the direction of pressure gradient ($t = 0.66$, Figure 4b). Acoustic waves consume the mean flow energy, while the wave propagates opposite to the direction of mean flow pressure gradient.

The vorticity generation term is negligible near the centerline, because vectors $\nabla\rho\prime$ and ∇P are almost collinear and their vector product is close to zero. The zero zone is bigger for the energy generation field than that for the vorticity generation (see Figure 4b): in addition to small vorticity, the first term in (21) is small as y is small and the second term is small as v is close to zero near symmetry line. Although vorticity is convected with the flow, generation of vorticity and, then, generation or decay of acoustic energy remain local phenomena.

To complete this section, we consider an acoustic dipole in the stagnation mean flow. Initial conditions correspond to a pair of positive and negative pulses (13) centered at $(0.25, 0.1)$ and $(0.25, -0.1)$. Pressure fields at $t = 0.33$ and $t = 0.66$ are presented in Figure 5. While waves propagate upstream of the mean flow, they become flat and their intensity behaves similar to that for the monopole source. The difference between dipole and monopole sources is that cancellation of waves for the dipole source leads to zero wave intensity near the centerline and formation of pressure quadrupoles.

4. Vorticity pulses. While an acoustic pulse travels with the speed of sound relative to a mean flow, the vorticity and entropy pulses convect with the mean flow. Therefore, in case B these pulses do not contribute to aeroacoustic noise and results are shown only in case A. Initial velocity field for considered vorticity pulse was first proposed by G. I. Taylor, cited in [9], and used by [6]:

$$\begin{aligned} u &= (y - y_c)\epsilon_v \exp\left[-d^2 \frac{(x - x_c)^2 + (y - y_c)^2}{a}\right], \\ v &= -(x - x_c)\epsilon_v \exp\left[-d^2 \frac{(x - x_c)^2 + (y - y_c)^2}{a}\right], \end{aligned} \tag{22}$$

where $\epsilon_v = 0.04, x_c = 0.25, y_c = 0$.

Vorticity and pressure field are shown in Figure 6. Initial vortex is strongly stretched by the stagnation flow and four pressure spots of alternating sign amplitude (quadrupole) are clearly seen in Figure 6a at $t = .42$. These spots elongate and become pressure waves that propagate outward (Figure 6b, $t = .62$). These waves remain invisible for an observer at the centerline; waves eventually become flat as we already observed for acoustic waves (Figure 6c, $t = .82$). According to Lighthill [11], the quadrupole radiation may have a much weaker far field in relation to its near field than even dipole radiation has; however, in cases without significant dipole and monopole sources the quadrupole may produce a significant noise.

In spite of the continuous stretching of the vortex, only waves emanating from the first quadrupole pressure spot were observed. To explore reasons for wave radiation, the stagnation mean flow has been switched off at $t = 0.5$ and, for $t > 0.5$, computations correspond to the static ambient conditions with already stretched vortex located near the wall. This situation holds when the vortex reaches the outer boundary of stagnation flow. The pressure fields at $t = 0.82$ and $t = 1.02$ are shown in Figure 7. The quadrupole wave source starts to form immediately after abrupt stop of vortex stretching (Figure 7a) and additional four waves radiate soon (Figure 7b). The similar phenomenon is observed for different switch-off time moments. These waves are weaker than that propagated in the stagnation flow as in the former case waves do not receive energy from the ambiance.

Acoustic radiation from a vorticity dipole in the stagnation flow is studied and results are shown in Figure 8. Initial conditions correspond to two counter-rotating vortices with velocity distribution (22) centered at $(0.25, 0.1)$ and $(0.25, -0.1)$. Each of the vortices is stretched along the wall outward the stagnation point and produces a quadrupole. Waves of the same sign merge near the centerline, and propagate upstream of the stagnation flow. Each of these two waves is surrounded by two waves of opposite sign. Therefore, the angular distribution of absolute value of wave amplitude has three maximums corresponding to a central wave and two peripheral waves.

5. Entropy pulses. Initial conditions for an entropy pulse are given by Eq.(13) for density and are equal to zero for pressure and velocities. In this case, an additional equation for pressure, which is equal to equation for density, is added to governing system (9) and solved numerically together with the other equations (see Section 2).

Results of computations are shown in Figure 9. Unlike the previously studied acoustic pulse, the entropy pulse does not spread and the area of density gradient remains localized. Therefore, in this case deposition of baroclinic vorticity produces a counter-rotating vortex pair (Figure 9b). Thus, the shape of obtained pressure waves for entropy monopole is expected to be similar to that for the vortical dipole. Actually, the second sound wave in Figure 9a is similar to sound waves in Figure 8b. In both cases, the symmetric centerline wave is surrounded by two symmetric waves of opposite sign. The difference between waves in these figures is due to the presence of initial density pulse superimposed with the induced vortex pair in the case of entropy pulse.

Combination of entropy and vortical pulses is studied as an example of interaction between initial vorticity and induced vortex pair. Initial conditions correspond to straightforward superposition of entropy and vorticity monopole pulses centered at $(0.25, 0)$. Radiation of opposite signed waves by a vorticity pulse interferes with radiation of the centerline symmetric wave by an entropy pulse (see Figure 10). Two cases with different relative strengths of entropy and vortical pulses are considered: a) pulse amplitudes are the same as in Eqs. (13, 22) (Figure 10a); b) initial amplitude of the entropy pulse is reduced twice (Figure 10b). In the former case, the reflected wave pattern deviates somewhat from the symmetric picture of the

pure entropy pulse wave pattern (compare Figures 10a and 9a). In the latter case alternating-sign spatially shifted pulses are clearly seen (compare Figures 10b and 6b).

6. Conclusions. Physics of propagation of monopole and dipole pulses in a stagnation flow in presence of solid wall is studied numerically.

It is shown that baroclinic deposition of vorticity due to non-zero vector product of mean pressure gradient and disturbance density gradient distinguishes disturbance propagation in a non-uniform flow from that in a uniform flow or in static ambient conditions. Generated vorticity serves as an agent to transfer energy between the mean flow and the disturbance. This results in amplification of acoustic waves propagating against the pressure gradient of the mean flow.

When an entropy monopole pulse propagates in a stagnation flow, the vorticity deposition produces a vortex pair and therefore, an entropy monopole radiates waves similar to those originated from a vorticity dipole.

Near-wall stretching of vorticity pulses by stagnation flow lead to radiation from a quadrupole. Numerical experiments in case of contiguous stretching by stagnation flow show the single generated quadrupole, whereas additional quadrupole may be generated by vortex freezing.

Obtained angular and planar distribution of wave amplitude may be useful for further far-field computations of radiated noise in presence of solid walls and non-uniform flows.

Acknowledgments. The author thanks Professor Geoffrey M. Lilley and Dr. Robert Rubinstein for discussion about aeroacoustics.

REFERENCES

[1] H. ATASSI AND J. GRZEDZINSKI, *Unsteady Disturbances of Streaming Motions around Bodies*, J. Fluid Mech., 209 (1989), pp. 385–403.

[2] G. K. BATCHELOR, *An Introduction to Fluid Mechanics*, Cambridge University Press, London, 1974.

[3] M. GOLDSTEIN, *Aeroacoustics*, McGraw-Hill, New York, 1976.

[4] M. E. GOLDSTEIN, *Unsteady Vortical and Entropic Distortions of Potential Flows round Arbitrary Obstacles* , J. Fluid. Mech., 89 (1978), pp. 433–468.

[5] J. HARDIN AND D. S. POPE, *A New Technique for Aerodynamic Noise Calculation*, in Proceedings of the DGLRR/AIAA 14th Aeroacoustics Conference, Washington, DC, 1992, pp. 448–456.

[6] J. C. HARDIN, J. R. RISTORCELLI, AND C. K. W. TAM, *ICASE/LaRC Workshop on Benchmark Problems in Computational Aeroacoustics*, Hampton, VA, 1995.

[7] C. HIRSCH, *Numerical Computation of Internal and External Flows, Vol. 1: Fundamentals of Numerical Discretizations*, John Wiley, Chichester, 1994.

[8] F. HU, *On Absorbing Boundary Conditions for Linearized Euler Equations by a Perfectly Matched Layer*, J. Comput. Phys., 129 (1996), pp. 262–281.

[9] O. INOUE AND Y. HATTORI, *Sound Generation by Shock-Vortex Interactions* , J. Fluid Mech., 380 (1999), pp. 81–116.

[10] S. K. LELE, *Compact Finite Difference Schemes with Spectral Like Resolution*, J. Comput. Phys., 103 (1992), pp. 16–42.

[11] J. LIGHTHILL, *Waves in Fluids*, Cambridge University Press, London, 1993.

[12] D. P. LOCKARD AND P. J. MORRIS, *The radiated noise from airfoils in realistic mean flows*, in Proceedings of the 35th Aerospace Sciences Meeting, Reno, NV, 1997. AIAA Paper 97-0286.

[13] T. D. NORUS, *Ground Impingement Noise of Supersonic Jets from Nozzles with Various Exit Geometries*, Journal of Aircraft, 29 (1992), pp. 993–998.

[14] W. A. OLSEN, J. H. MILES, AND R. G. DORSCH, *Noise Generated by Impingement of a Jet upon a Large Flat Board*, NASA TN D-7075, 1972.

[15] S. SLIMON, M. SOTERIOU, AND D. DAVIS, *Computational Aeroacoustics Simulations Using the Expansion about Incompressible Flow Approach*, AIAA Journal, 37 (1999), pp. 409–416.

[16] P. T. SODERMAN, *The Prediction of STOLV Noise: Current Semi-Empirical Methods and Comparisons with Jet Noise Data*, SAE Transactions, 99 (1990), pp. 307–335.

[17] C. K. W. TAM AND Z. DONG, *Wall Boundary Conditions for High-Order Finite-Difference Schemes in Computational Aeroacoustics*, Theoretical and Computational Fluid Dynamics, 6 (1994), pp. 303–322.

[18] J. WILLIAMSON, *Low Storage Runge-Kutta Schemes*, J. Comput. Phys., 35 (1980), pp. 48–56.

[19] R. V. WILSON, A. O. DEMUREN, AND M. CARPENTER, *High-Order Compact Schemes for Numerical Simulation of Incompressible Flows*, ICASE Report No. 98-13, 1998.

[20] J. YANG, T. KUBOTA, AND E. ZUKOSKI, *A Model for Characterization of a Vortex Pair Formed by Shock Passage over a Light-Gas Inhomogeneity*, Journal of Fluid Mechanics, 258 (1994), pp. 81–116.

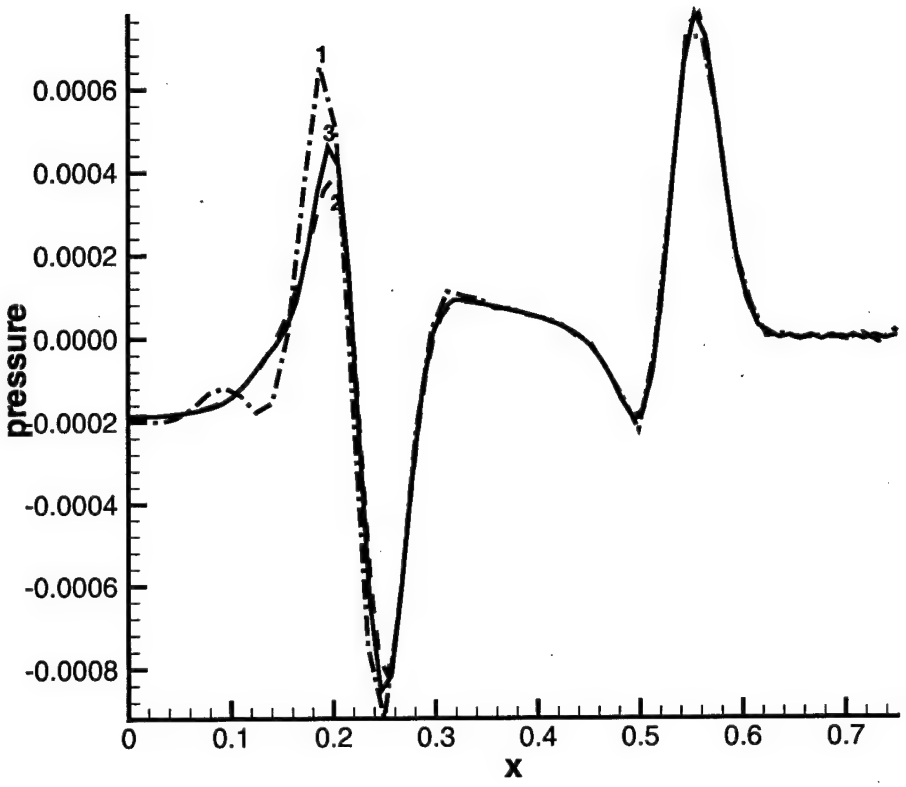

FIG. 1. *Centerline pressure for acoustic pulse in stagnation flow at* $t = 0.5$. *Numerical grids: 1)* 80×80; *2)* 120×120; *3)* 160×160.

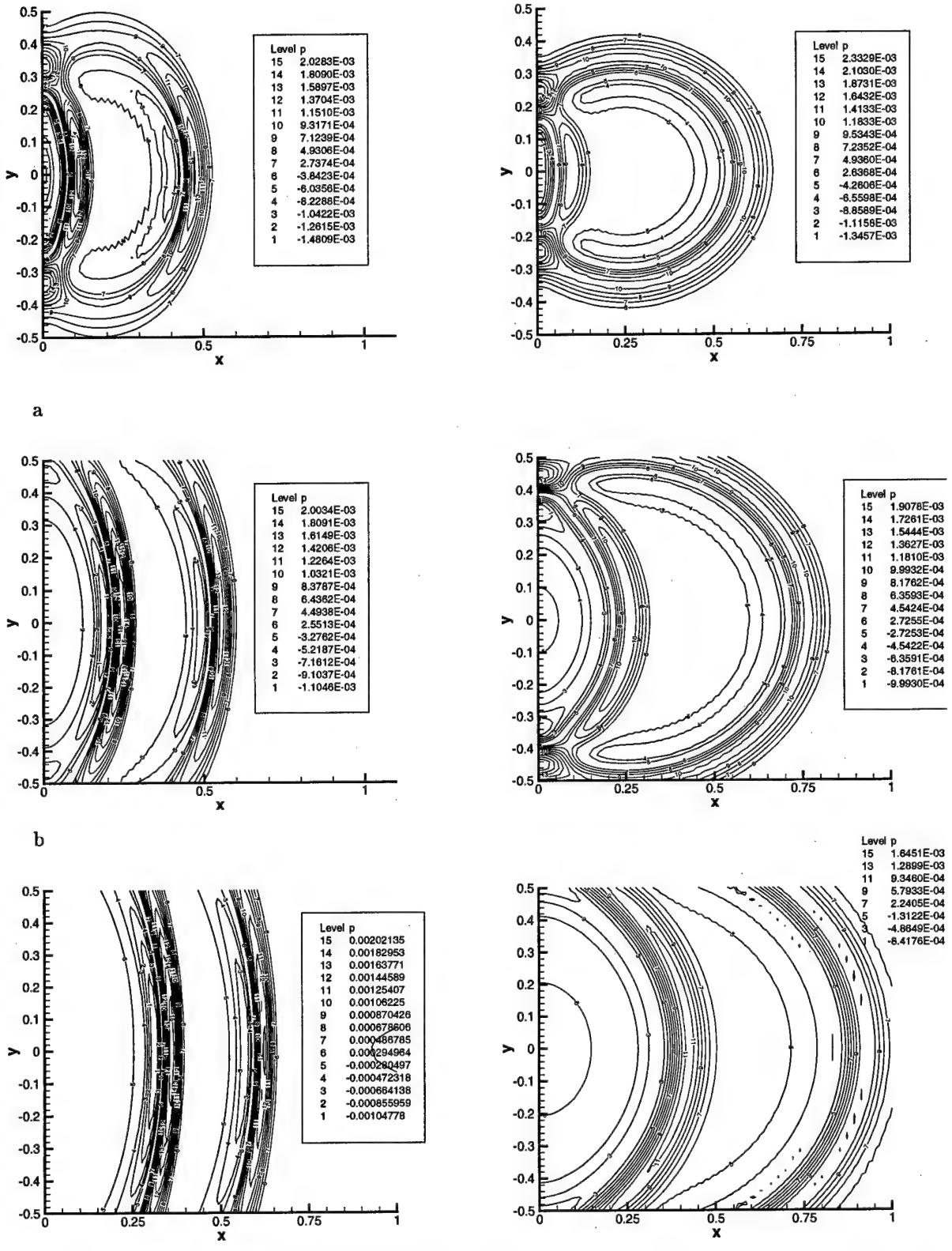

FIG. 2. *Acoustic pulse propagation in stagnation mean flow (case A, left column) and in static ambient conditions (case B, right column). Acoustic pressure isolines are taken with 15 equally spaced intervals between maximum and minimum. Times: a) .33; b) .49; c) .66.*

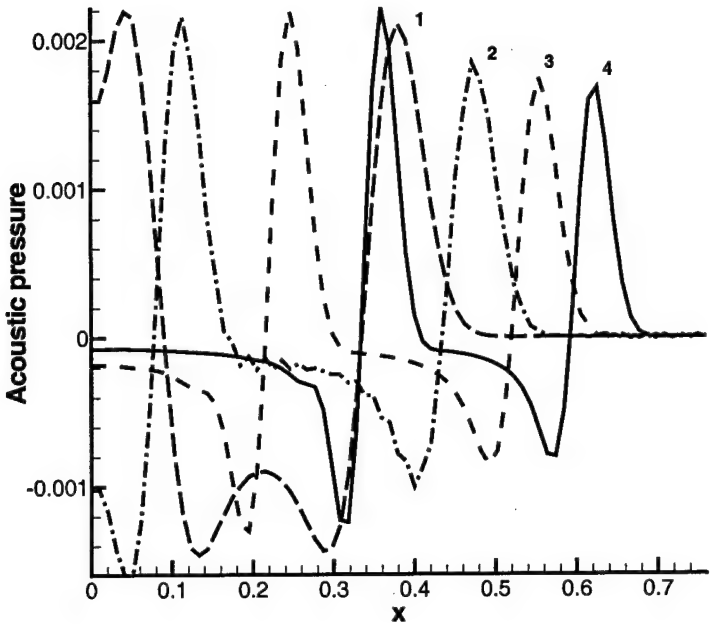

a

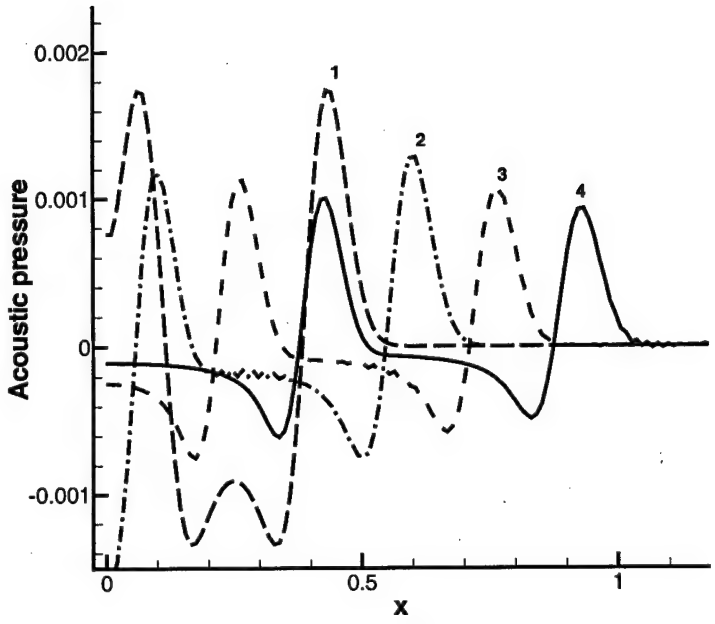

b

FIG. 3. *Acoustic pressure profile along the symmetry axis: a) stagnation mean flow, case A; b) static ambient conditions, case B. Times: 1)* $t = 0.17$; *2)* $t = 0.33$; *3)* $t = 0.49$; *4)* $t = 0.66$.

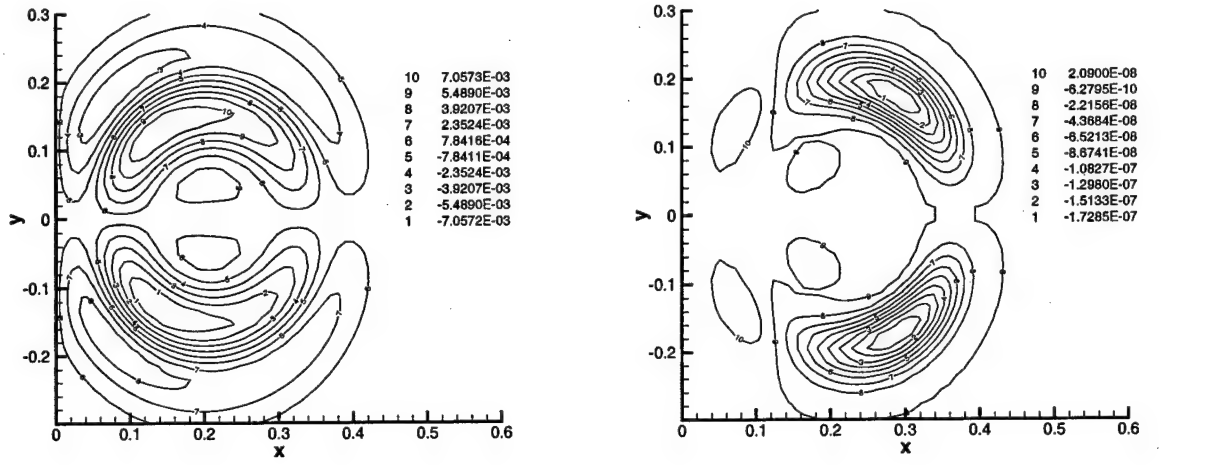

a

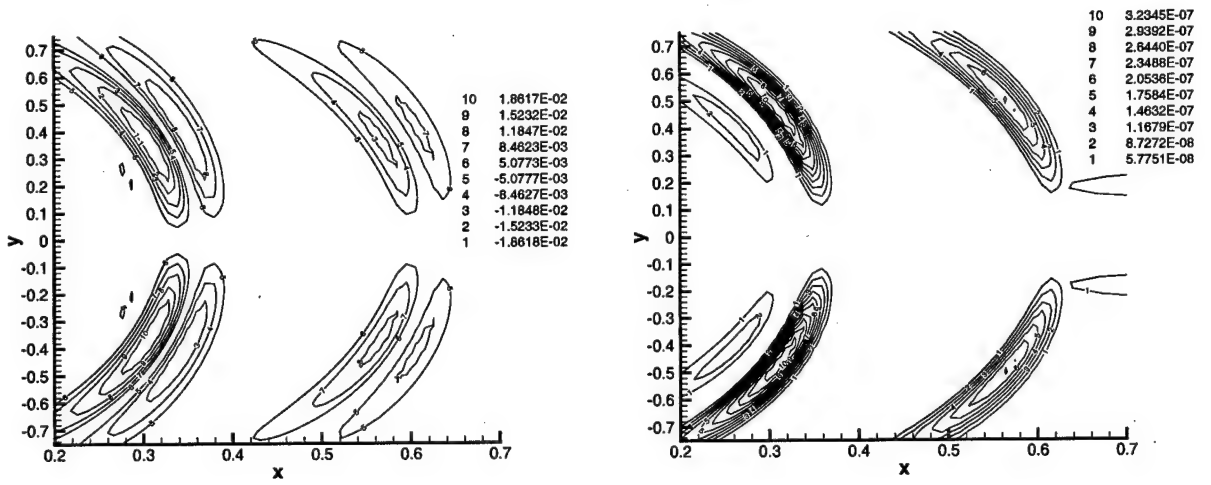

b

FIG. 4. *Vorticity generation (left column) and acoustic energy generation (right column). Isolines are taken with 10 equally spaced intervals between maximum and minimum. Times: a)* $t = 0.17$; *b)* $t = 0.66$.

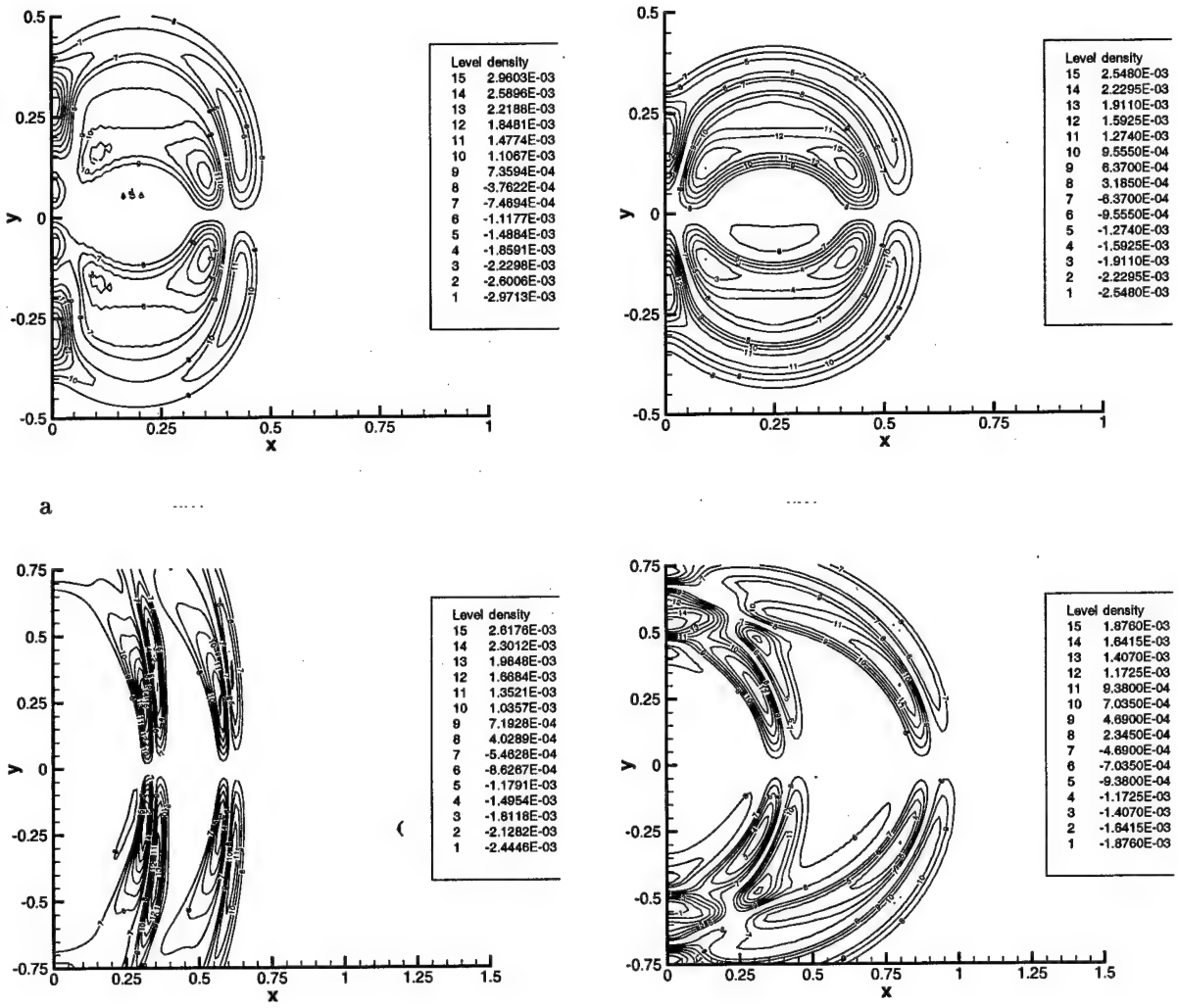

FIG. 5. *Waves originated from acoustic dipole. Left column is the stagnation flow (case A) and right column is the static ambiant conditions (case B). Time moments: a) $t = 0.33$; b) $t = 0.66$.*

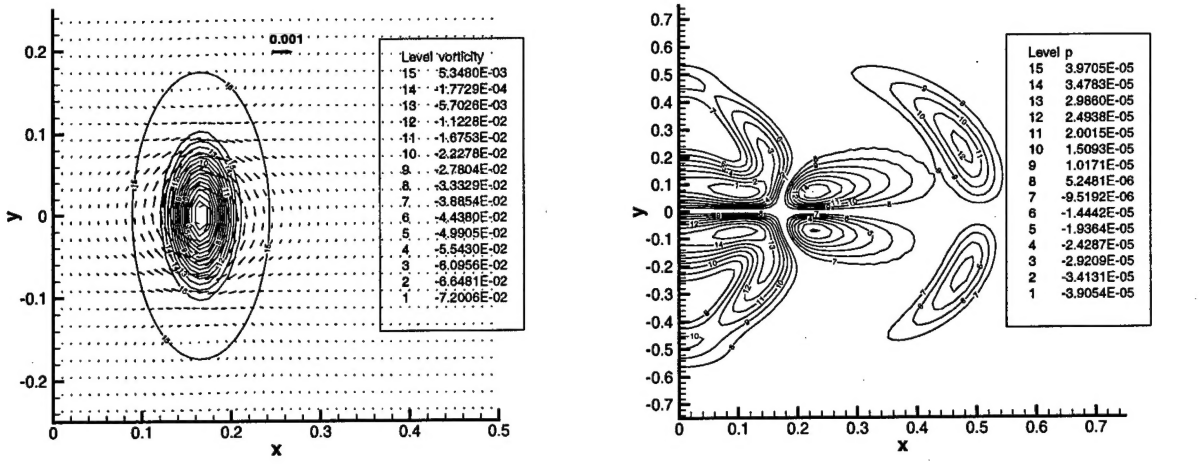

a

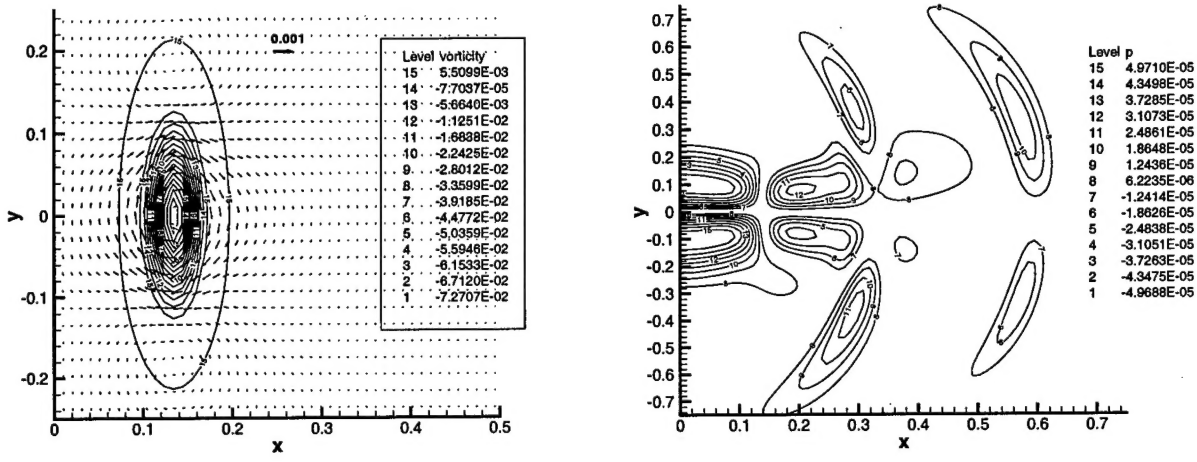

b

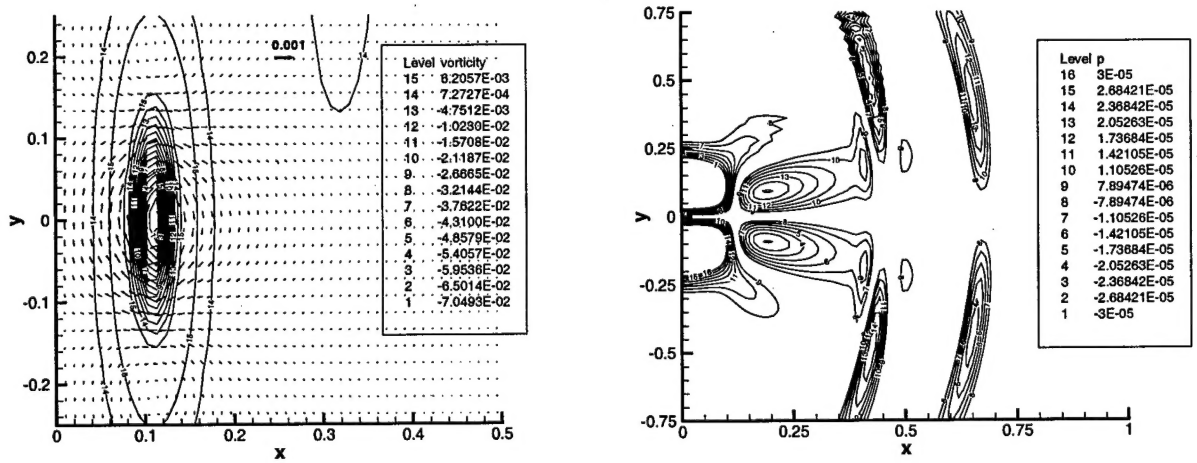

c

FIG. 6. *Propagation of vortical disturbance in the mean stagnation flow. Left column-vorticity field; right columns-pressure field. Time moments: a) .42; b) .62; c) .82.*

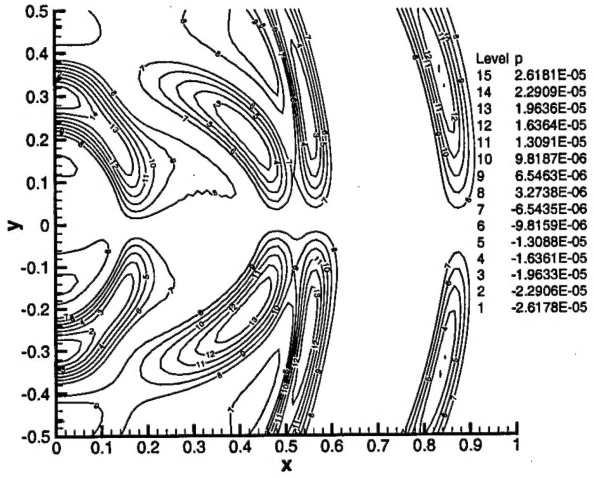

a

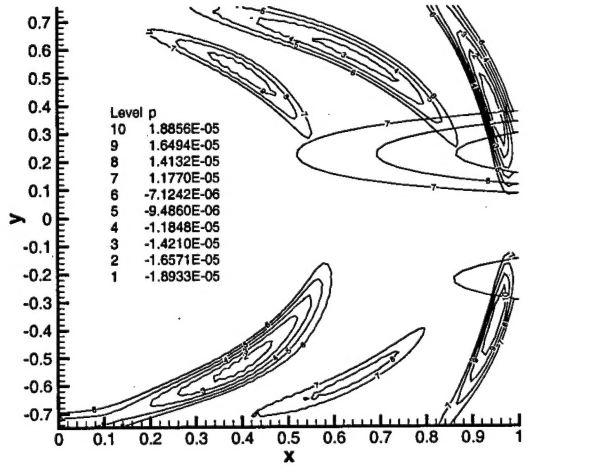

b

FIG. 7. *Waves originated from the stretched near-wall vortex. in the static ambiance. Stagnation mean flow has been switched-off at* $t = 0.5$ *and pressure fields are shown at the following time moments: a) 0.82; b) 1.03.*

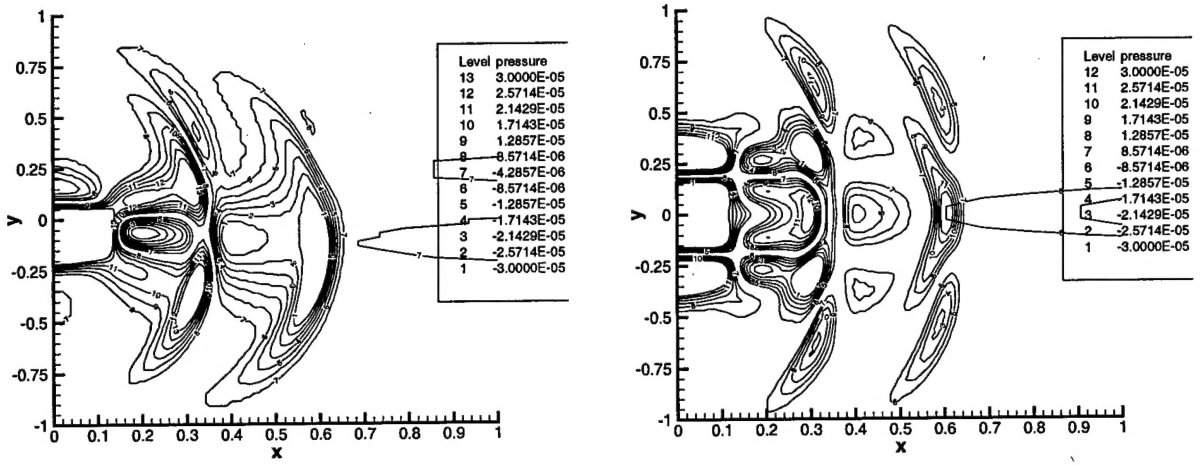

a b

FIG. 8. *Pressure field originated from vorticity dipole in stagnation flow. Time moments: a) $t = 0.32$; b) $t = 0.66$.*

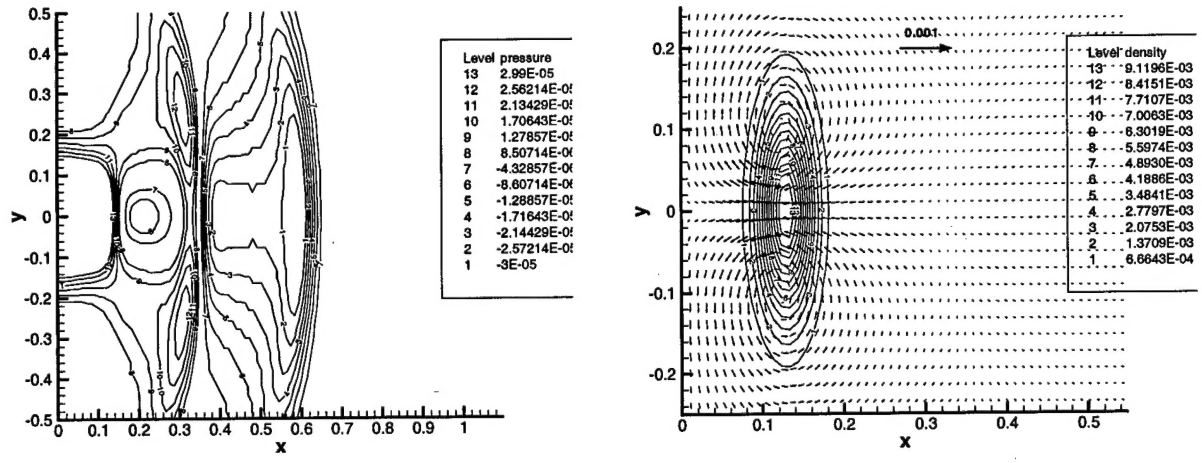

a b

FIG. 9. *Acoustic field originated from entropy pulse: a) pressure field; b) density field and velocity vector at $t = 0.66$. Reference vector $\bar{u} = 0.001$ is shown.*

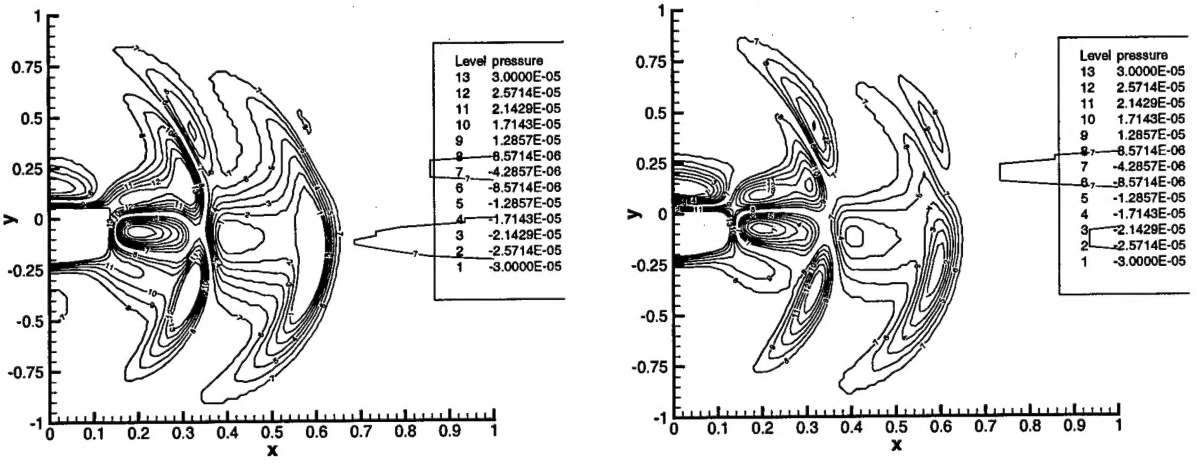

FIG. 10. *Combined entropy and vorticity pulse. Time moment* $t = 0.66$. *Intensity of entropy pulse: a)* $a = 0.01$; *b)* $a = 0.005$.